NASA/CR-1998-207680
ICASE Report No. 98-18

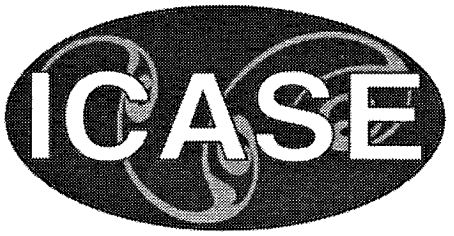

Optimal Control of Unsteady Stokes Flow Around a Cylinder and the Sensor/Actuator Placement Problem

Josip Loncaric
ICASE, Hampton, Virginia

Institute for Computer Applications in Science and Engineering
NASA Langley Research Center
Hampton, VA

Operated by Universities Space Research Association

National Aeronautics and
Space Administration

Langley Research Center
Hampton, Virginia 23681-2199

Prepared for Langley Research Center under
Contracts NAS1-19480 and NAS1-97046

May 1998

Available from the following:

NASA Center for AeroSpace Information (CASI)
7121 Standard Drive
Hanover, MD 21076-1320
(301) 621-0390

National Technical Information Service (NTIS)
5285 Port Royal Road
Springfield, VA 22161-2171
(703) 487-4650

OPTIMAL CONTROL OF UNSTEADY STOKES FLOW AROUND A CYLINDER AND THE SENSOR/ACTUATOR PLACEMENT PROBLEM

JOSIP LONČARIĆ*

Abstract

Abstract. Effective placement of sensors and actuators is of crucial importance in flow control. Instead of using combinatorial search to identify optimal locations, we pose a related problem of polynomial complexity. If one could sense everything and actuate everywhere, what should one do? Using the unsteady 2D Stokes flow around a cylinder as an example, we obtain the analytic solution of an optimal distributed control problem and describe its spatial structure. At low circumferential wavenumbers or close to the cylinder wall, boundary vortex generators are shown to be more effective than colocated vorticity damping. This analytic solution has also been used to test numerical methods, demonstrating the importance of using discretization which resolves all eigenfunctions of interest.

Key words. optimal flow control, exterior Stokes flow, sensor/actuator placement, design

Subject classification. Applied and Numerical Mathematics, Controls

1. Introduction. Given the task of controlling a physical system described by partial differential equations, one must first select sensors and actuators, then devise a controller for the resulting distributed system. Although intuition and experience can sometimes help in the design stage, this approach fails when prior experience is lacking. Confronted with a radically different problem, such as the possibility of using several small sensors and actuators, one quickly finds that the number of possible configurations grows combinatorially. For example, [11] investigated the design optimization problem of placing $M = 8$ active struts into a structure with $N = 1507$ possible locations, resulting in a discrete search space of approximately 6.5×10^{20} possible designs. The search space grows dramatically as either N or M is increased.

While this formulation of the problem may be natural in structures composed of discrete components such as struts, a different approach is needed in continuum problems where the number of candidate locations is potentially infinite. We shall adopt the point of view that the search space for placement of sensors and actuators may be reduced by performing a thought experiment in optimal control. This thought experiment asks the following question: *If one could sense everything and control everything, what should one do?*

While distributed control is typically not feasible, it leads to the optimal design which we can try to approximate by feasible designs. We anticipate that the optimal feedback law favors some spatial regions over others. This can happen if the system dynamics exhibit spatially localized behavior, such as boundary layers in flow control problems, or through a particular choice of the optimality criterion. In either case, we espect that the optimal distributed feedback law will be of the form

$$u(a) = -\int_{\Omega} \kappa(a,s)x(s)ds \tag{1.1}$$

where $u(a)$ is the optimal control input at each actuation location a in Ω, $x(s)$ is the state variable at sensing location s, $\kappa(a,s)$ is the optimal feedback kernel and the integral ranges over the entire volume of the domain

*ICASE, M/S 403, NASA Langley Research Center, Hampton, VA 23681-2199. E-mail: *josip@icase.edu.* This research was partially supported by the National Aeronautics and Space Administration under NASA Contract Nos. NAS1-19480 and NAS1-97046 while the author was in residence at the Institute for Computer Applications in Science and Engineering (ICASE), M/S 403, NASA Langley Research Center, Hampton, VA, 23681-2199.

Ω. As observed by [1, 12], this integral may be approximated by neglecting the pairs of locations for which $\kappa(a,s)$ is small. The remaining pairs of locations where $\kappa(a,s)$ is large define a reduced design search space. The thought experiment can also be applied recursively, until the search for feasible and cost effective designs becomes manageable.

Prior work on this problem focused on controllability and observability for distributed parameter systems, leading to to the concept of *strategic actuators and sensors* [5, 6]. This property can be completely discontinuous. For the heat equation on the unit interval, a point actuator or sensor is strategic if and only if its coordinate is an irrational number.

The computational method introduced in [10] is most suitable for design problems where a small set of candidate locations is already heuristically determined. Combinatorial growth of computational complexity is avoided by restricting attention to candidate sensor/actuator pairs. The *pairwise* dimensions of the intersection of controllable and observable subspaces are computed first, and pairs are ranked in terms of effectiveness and versatility. For each significant vibration mode of the testbed structure, the best pairs were chosen based on a combined index defined in terms of the controllability and observability Gramians.

Computing the optimal $\kappa(a,s)$ in (1.1) also leads to a problem of polynomial complexity, but without initial assumptions about candidate locations. Given a discretization of space into N^3 locations, the linearized dynamics can be described by a $N^3 \times N^3$ matrix and the optimal feedback found in at most $O(N^9)$ steps. By contrast, in placing M sensors or actuators the discrete search approach would require the evaluation of

$$\frac{N^3!}{M!(N^3-M)!} \approx 2.8 \times 10^{53} \tag{1.2}$$

possible designs when $N = 100$ and $M = 10$. The cost of computing the optimal feedback kernel is much lower, of order $N^9 = 10^{18}$. While not completely impossible, this is still daunting even in 2D problems, where the computational cost would be of order $N^6 = 10^{12}$. Further reduction of computational complexity is needed.

Instead of reducing spatial resolution, we shall focus on constructing a reduced order model of a particular system. We shall seek to construct a sequence of reduced order models by using a modal approximation. This approach may be rigorously justified provided that the system belongs to the class of *spectral systems* defined in [2, 3]. In fact, we shall show how system dynamics of the unsteady Stokes flow around a cylinder may be diagonalized, derive the exact optimal feedback kernel, and then construct its analytic approximation whose worst case performance loss is less than 0.026 percent. We begin by formulating the problem.

2. Exterior Stokes flow problem. Much of our understanding of the full Navier-Stokes equations begins with the Stokes flow, which represents their linearization around the motionless state [13]. Incompressible fluid dynamics can be thought of as the response of the Stokes flow to forcing by the nonlinear term. While the nonlinear term conserves the kinetic energy, a vorticity perturbation can grow via the vortex stretching mechanism in 3D. In 2D, this mechanism is absent and the vorticity is conserved along particle paths when viscosity and forcing are neglected. Consequently, the total enstrophy $\frac{1}{2}\|\omega\|^2$ cannot increase under the action of the nonlinear term alone [7]. Instead, additional vorticity is created at the solid boundaries in a process governed by the viscous sublayer and the Stokes flow equations. A correct understanding of the boundary-fluid interaction becomes particularly significant when boundary control is contemplated.

The flow of incompressible viscous fluid around a cylinder is a prototype exterior flow problem. For control purposes at low Reynolds numbers, vorticity creation at the solid boundaries and viscous dissipation are the two physical processes of primary importance, while the conservative nonlinear term is secondary.

This suggests that a simpler model in which the nonlinear term is neglected would still capture the essential aspects of this flow control problem.

Consider the corresponding 2D Stokes flow in streamfunction representation described by the equations

$$\mathbf{v} = -\hat{\mathbf{z}} \times \vec{\nabla}\psi \tag{2.1}$$

$$\omega = \vec{\nabla} \times \mathbf{v} = -\Delta\psi \tag{2.2}$$

$$\frac{\partial \omega}{\partial t} = \Delta\omega \tag{2.3}$$

where ψ is the streamfunction whose gradient rotated by $-\pi/2$ is the velocity field $\mathbf{v}$. The boundary conditions are

$$\psi|_{r=1} = 0 \tag{2.4}$$

$$\left.\frac{\partial \psi}{\partial r}\right|_{r=1} = 0 \tag{2.5}$$

$$\lim_{r\to\infty} \vec{\nabla}\psi = 0 \tag{2.6}$$

As is customary in 2D flows, the velocity $\mathbf{v}$ will be thought of as a 2-vector but ψ and the vorticity ω will be considered scalars. Moreover, we shall interpret $\mathbf{v}$ as a finite energy flow perturbation.

At this point it is useful to note that the scalar second order elliptic equation $\Delta\psi = -\omega$ must satisfy more than two boundary conditions, which is only possible if the vorticity ω satisfies certain integral compatibility conditions. As pointed out by [9], this compatibility is achieved by the creation of vortex sheets at the solid boundary. This vorticity creation process at the wall couples to the exterior flow through viscosity, diffusing the vortex sheet outwards in an arbitrarily short time. While the implicitly created vortex sheets involve delta functions which present a challenge to numerical approximations, we intend to consider a family of reduced order models which approximate the full dynamics by neglecting the highly stable modes. As we shall show later, the retained modes can be expressed analytically in terms of smooth functions which can be approximated numerically without much difficulty.

We are interested in flows for which the initial vorticity is contained within the computational domain of radius R and the diffusion of vorticity across the artificial boundary $r = R$ is negligible. To that end, let us introduce coordinate variables $\rho = \log(r)$ and θ, then apply the Fourier transform in the θ direction. The relevant operators may be written as follows:

$$\vec{\nabla} = \frac{1}{r}\begin{bmatrix} \frac{\partial}{\partial\rho} \\ \frac{\partial}{\partial\theta} \end{bmatrix} = \frac{1}{r}\begin{bmatrix} \frac{d}{d\rho} \\ ik \end{bmatrix} \tag{2.7}$$

$$\Delta = \frac{1}{r^2}\left(\frac{\partial^2}{\partial\rho^2} + \frac{\partial^2}{\partial\theta^2}\right) = \frac{1}{r^2}\left(\frac{d}{d\rho} - |k|\right)\left(\frac{d}{d\rho} + |k|\right) \tag{2.8}$$

This factorization of the Laplacian in Fourier representation separates the modes which grow and decay as $r \to \infty$. In complex analysis, this is equivalent to the Wiener-Hopf factorization, which has been used to study boundary layer growth near the leading edge of a flat plate [8], but it will also prove useful in our 2D problem. We note that this approach generalizes to higher dimensions via the Calderon projector [15].

As shown in [14] for the problem $\Delta u = f$, whenever the forcing f vanishes outside the computational domain, the boundary condition $u \to 0$ at infinity is *exactly* represented by the countably many conditions

$$\left(\frac{d}{d\rho} + |k|\right) u_k(\rho)\Big|_{\rho=\log(R)} = 0, \qquad k = 0, \pm 1, \pm 2, \ldots \tag{2.9}$$

$$u_0(\log(R)) = 0 \tag{2.10}$$

applied at the artificial boundary of the computational domain. These boundary conditions are nonlocal and are best applied in the Fourier representation.

3. Pseudodifferential representation. Let us also introduce the following *pseudodifferential representation.*

DEFINITION 3.1. *The pseudodifferential representation ξ of the flow state with the streamfunction ψ is given by*

$$\xi_k(\rho) = \frac{1}{r}\left(\frac{d}{d\rho} + |k|\right)\psi_k(\rho). \tag{3.1}$$

This definition implies that

$$\xi_k(\rho) = -v_k^\theta(\rho) - i\,\mathrm{sgn}(k) v_k^r(\rho) \tag{3.2}$$

where v^θ and v^r are the circumferential and radial components of the solenoidal velocity field, respectively. We note that ξ is a real scalar field. Moreover, unlike the streamfunction or vorticity, ξ scales with velocity as the physical length scale is changed.

THEOREM 3.2. *Given a function $\xi_k(\rho)$, the streamfunction $\psi_k(\rho)$ is*

$$\psi_k(\rho) = \int_0^\rho e^{-|k|(\rho-\sigma)}\xi_k(\sigma)e^\sigma d\sigma \tag{3.3}$$

$$= \int_1^r \left(\frac{s}{r}\right)^{|k|} \xi_k(\log(s))ds\ . \tag{3.4}$$

The proof follows by application of the variation of constants formula and the fact that the solid boundary $r = 1$ is the streamline $\psi = 0$.

Furthermore, $v_k(\rho) = 0$ clearly implies that $\xi_k(\rho) = 0$. The converse need not be true since $\xi_k(\rho) = 0$ implies only that $v_k^\theta(\rho) = -i\,\mathrm{sgn}(k)v_k^r(\rho)$ which has nonzero solenoidal solutions derived from corner flows $\psi_k = 1/r^{|k|}$ for $r \geq R$. However, as an easy consequence of the above theorem, we conclude that when ξ vanishes outside a bounded domain, $\mathbf{v}$ decays to zero at infinity.

COROLLARY 3.3. *Whenever the support of ξ is contained within a bounded domain $r < R$, the corresponding flow field satisfies the boundary condition $\mathbf{v} \to 0$ at infinity.*

We can now prove a stronger result which holds even when ξ does not have compact support.

THEOREM 3.4. *The following boundary conditions on ξ and $\mathbf{v}$ at infinity are equivalent for continuous functions ξ:*

$$\lim_{\rho\to\infty} \xi = 0 \Longleftrightarrow \lim_{\rho\to\infty} \mathbf{v} = 0. \tag{3.5}$$

The implication $\Leftarrow$ is a trivial consequence of the definition of ξ. To obtain the implication $\Rightarrow$, note that the velocity field is linear in ξ. Let us write $\xi = \xi_0 + \xi_\infty$ where the ξ_∞ vanishes for $\rho < \log(R)$ and ξ_0 vanishes for $\rho \geq \log(R)$. The corresponding solenoidal velocity field is $\mathbf{v} = \mathbf{v}_0 + \mathbf{v}_\infty$ where $\mathbf{v}_0$ decays to zero at infinity by the previous corollary. For $\mathbf{v}_\infty$ we use the boundary condition $\psi = 0$ at $r = 1$ to obtain the Fourier coefficients of the radial velocity

$$v_{\infty,k}^r(\rho) = \frac{i\,k}{r}\psi_k(\rho) \tag{3.6}$$

$$= \frac{i\,k}{e^{\rho}} \int_0^{\rho} e^{-|k|(\rho-\sigma)} e^{\sigma} \xi_{\infty,k}(\sigma) d\sigma \tag{3.7}$$

$$= i\,k \int_{\log(R)}^{\rho} e^{-(|k|+1)(\rho-\sigma)} \xi_k(\sigma) d\sigma \tag{3.8}$$

for $\rho > \log(R)$. Since ξ decays to zero at infinity, define $\epsilon(k,R)$ by

$$\epsilon(k,R) = \sup_{\rho \geq \log(R)} |\xi_k(\rho)| \tag{3.9}$$

which leads to the inequality

$$|v^r_{\infty,k}(\rho)| \leq \epsilon(k,R)|k| \int_{\log(R)}^{\rho} e^{-(|k|+1)(\rho-\sigma)} d\sigma. \tag{3.10}$$

Taking the limit $\rho \to \infty$, we obtain

$$\lim_{\rho\to\infty} |v^r_{\infty,k}(\rho)| \leq \epsilon(k,R) \frac{|k|}{|k|+1} < \epsilon(k,R) \tag{3.11}$$

which holds for all k, R. Since ξ is continuous, its Fourier series converges absolutely and uniformly, and so does the Fourier series for v^r_{∞}. Given that $\xi \to 0$ at infinity, the conclusion $v^r \to 0$ follows by taking the limit $R \to \infty$. From the definition of ξ_k we then obtain that the tangential component $v^{\theta} \to 0$ and the proof is complete.

At this point the main advantage of the pseudodifferential representation has become clear. We shall represent flows in terms of ξ, where ξ satisfies Dirichlet boundary conditions. By contrast, the velocity-vorticity and the streamfunction-vorticity representations involve the difficulty of determining the vorticity created at the solid boundary.

While the pseudodifferential representation has been defined in terms of its Fourier coefficients, an equivalent physical interpretation in terms of singular integral operators can be found. The resulting equations explicitly demonstrate the non-local nature of the pseudodifferential representation.

THEOREM 3.5. *Given a smooth streamfunction ψ, the pseudodifferential representation ξ is given in terms of physical coordinates by*

$$\xi(\rho,\theta) = \frac{1}{r}\left(\frac{\partial \psi(\rho,\theta)}{\partial \rho} + \frac{1}{\pi} \int_0^{2\pi} \frac{\partial^2 \psi(\rho,\theta-\phi)}{\partial \theta^2} \log\left|\sin\frac{\phi}{2}\right| d\phi \right). \tag{3.12}$$

The proof follows by applying the convolution theorem to the terms in the integral and integrating by parts, since the function $-2\log|\sin(x/2)|$ has Fourier coefficients $1/|k|$ for nonzero k. For nonsmooth ψ, this equality may still be interpreted in the sense of distributions, or taken as an alternative definition of ξ. This result can also be expressed in terms of the velocity fields.

COROLLARY 3.6. *The pseudodifferential representation ξ is related to smooth divergence-free velocity fields by*

$$\xi(\rho,\theta) = -v^{\theta}(\rho,\theta) + \frac{1}{\pi} \int_0^{2\pi} \frac{\partial v^r(\rho,\theta-\phi)}{\partial \theta} \log\left|\sin\frac{\phi}{2}\right| d\phi. \tag{3.13}$$

4. Reformulated Stokes flow problem. Besides the field ξ, we define the following three operators

$$\mathcal{R}f(\rho) = rf(\rho) \tag{4.1}$$

$$\mathcal{B}_{|k|}f_k(\rho) = \left(\frac{d}{d\rho} - |k|\right) f_k(\rho) \tag{4.2}$$

$$\mathcal{F}_{|k|}f_k(\rho) = \left(\frac{d}{d\rho} + |k|\right) f_k(\rho) \tag{4.3}$$

and their particular inverses

$$\mathcal{R}^{-1}f_k(\rho) = \frac{f_k(\rho)}{r} \tag{4.4}$$

$$\mathcal{B}_{|k|}^{-1}f_k(\rho) = -\int_\rho^\infty e^{-|k|(\sigma-\rho)} f_k(\sigma)d\sigma \tag{4.5}$$

$$\mathcal{F}_{|k|}^{-1}f_k(\rho) = \int_0^\rho e^{-|k|(\rho-\sigma)} f_k(\sigma)d\sigma. \tag{4.6}$$

Given these definitions, the factorization (2.8) of the Laplacian may be compactly written as

$$\Delta_{|k|}f_k(\rho) = \mathcal{R}^{-2}\mathcal{B}_{|k|}\mathcal{F}_{|k|}f_k(\rho). \tag{4.7}$$

We shall also be using the commutativity properties

$$\mathcal{B}_{|k|+a}\mathcal{R}^a = \mathcal{R}^a\mathcal{B}_{|k|} \tag{4.8}$$

$$\mathcal{F}_{|k|}\mathcal{R}^a = \mathcal{R}^a\mathcal{F}_{|k|+a} \tag{4.9}$$

$$\mathcal{B}_a\mathcal{F}_b = \mathcal{F}_b\mathcal{B}_a\ . \tag{4.10}$$

While the above definitions are given in terms of Fourier components, physical interpretation of these operators can be found. The following theorem is an easy consequence of the convolution theorem once we observe that for positive σ the Fourier coefficients $e^{-|k|\sigma}$ represent the function

$$g(\sigma,\phi) \stackrel{\text{def}}{=} \frac{\sinh(\sigma)}{\cosh(\sigma) - \cos(\phi)} \quad \text{for } \sigma > 0 \tag{4.11}$$

whose limit as $\sigma \to 0^+$ has all Fourier coefficients equal to 1 provided that it is defined to be

$$g(0,\phi) \stackrel{\text{def}}{=} \pi\,\delta(\sin(\phi/2)). \tag{4.12}$$

The function $g(\sigma,\phi)$ may be recognized as the Poisson kernel.

THEOREM 4.1. *The above operators and their particular inverses have the following physical representations:*

$$\mathcal{R} : f(\rho,\theta) \mapsto r\,f(\rho,\theta) \tag{4.13}$$

$$\mathcal{R}^{-1} : f(\rho,\theta) \mapsto \frac{f(\rho,\theta)}{r} \tag{4.14}$$

$$\mathcal{B} : f(\rho,\theta) \mapsto \frac{\partial f(\rho,\theta)}{\partial\rho} - \frac{1}{2\pi}\int_0^{2\pi} \frac{\partial^2 f(\rho,\theta-\phi)}{\partial\theta^2} h(\phi)d\phi \tag{4.15}$$

$$\mathcal{B}^{-1} : f(\rho,\theta) \mapsto -\int_0^\infty \frac{1}{2\pi}\int_0^{2\pi} g(\sigma,\phi) f(\rho+\sigma,\theta-\phi)\,d\phi\,d\sigma \tag{4.16}$$

$$\mathcal{F} : f(\rho,\theta) \mapsto \frac{\partial f(\rho,\theta)}{\partial\rho} + \frac{1}{2\pi}\int_0^{2\pi} \frac{\partial^2 f(\rho,\theta-\phi)}{\partial\theta^2} h(\phi)d\phi \tag{4.17}$$

$$\mathcal{F}^{-1} : f(\rho,\theta) \mapsto \int_0^\rho \frac{1}{2\pi}\int_0^{2\pi} g(\sigma,\phi) f(\rho-\sigma,\theta-\phi)\,d\phi\,d\sigma \tag{4.18}$$

where $r = e^{\rho}$, $h(\phi) = \log\left(4\sin(\phi/2)^2\right)$ *and* $g(\sigma, \phi)$ *is defined as above.*

After shortening the notation by making the dependence on ρ implicit, the model problem is described by the following theorem:

THEOREM 4.2. *The pseudodifferential representation of the Stokes flow around a cylinder is described by the following equations:*

$$\psi_k = \mathcal{F}_{|k|}^{-1}\mathcal{R}\xi_k \tag{4.19}$$

$$\omega_k = -\mathcal{R}^{-1}\mathcal{B}_{|k|-1}\xi_k \tag{4.20}$$

$$v_k^r = \frac{i\,\mathrm{sgn}(k)}{2}\mathcal{R}^{-1}\left(\mathcal{F}_{|k|} - \mathcal{B}_{|k|}\right)\psi_k = i\,k\mathcal{F}_{|k|+1}^{-1}\xi_k \tag{4.21}$$

$$v_k^\theta = \frac{1}{2}\mathcal{R}^{-1}\left(\mathcal{B}_{|k|} + \mathcal{F}_{|k|}\right)\psi_k = \left(|k|\mathcal{F}_{|k|+1}^{-1} - \mathcal{I}\right)\xi_k \tag{4.22}$$

$$\frac{d\xi_k}{dt} = \mathcal{R}^{-2}\mathcal{F}_{|k|-1}\mathcal{B}_{|k|-1}\xi_k = \Delta_{||k|-1|}\xi_k \tag{4.23}$$

with Dirichlet boundary conditions on ξ_k.

Equation (4.19) follows from the definition of ξ and the boundary condition $\psi = 0$ at $r = 1$. Equations (4.21) and (4.22) also follow immediately. The equation (4.20) is verified as follows:

$$\omega_k = -\Delta\psi_k \tag{4.24}$$

$$= -\mathcal{R}^{-2}\mathcal{B}_{|k|}\mathcal{F}_{|k|}\psi_k \tag{4.25}$$

$$= -\mathcal{R}^{-1}\mathcal{B}_{|k|-1}\mathcal{R}^{-1}\mathcal{F}_{|k|}\psi_k \tag{4.26}$$

$$= -\mathcal{R}^{-1}\mathcal{B}_{|k|-1}\xi_k. \tag{4.27}$$

This result shows that whenever ξ vanishes for $r \geq R$, so does ω. Conversely, given the boundary condition $\mathbf{v} \to 0$ at infinity, one may invert the equation (4.20) and show that whenever ω vanishes for $r \geq R_\omega$, so does ξ. Both properties are desirable given the bounded computational domain.

Assuming that the initial vorticity distribution is contained within a smaller domain $r \leq R_\omega < R$, diffusion of vorticity out of the computational domain is insignificant for $t \ll (R - R_\omega)^2$. By choosing $R \gg R_\omega + \sqrt{T}$ this reformulated problem can be made applicable for all $t \leq T$. Provided that the initial disturbance decays to almost zero by the time $t = T$, the forcing at the artificial boundary $r = R$ will again be negligible. In the limit $R \to \infty$, the pseudodifferential representation satisfies the the equivalent boundary conditions over the entire exterior domain.

Finally, equation (4.23) is obtained from (2.3) as follows:

$$\frac{\partial\omega}{\partial t} = \Delta\omega \tag{4.28}$$

$$\mathcal{R}^{-1}\mathcal{B}_{|k|-1}\frac{d\xi_k}{dt} = \mathcal{R}^{-2}\mathcal{B}_{|k|}\mathcal{F}_{|k|}\mathcal{R}^{-1}\mathcal{B}_{|k|-1}\xi_k \tag{4.29}$$

$$\mathcal{B}_{|k|-1}\frac{d\xi_k}{dt} = \mathcal{R}^{-1}\mathcal{B}_{|k|}\mathcal{F}_{|k|}\mathcal{R}^{-1}\mathcal{B}_{|k|-1}\xi_k \tag{4.30}$$

$$\mathcal{B}_{|k|-1}\frac{d\xi_k}{dt} = \mathcal{B}_{|k|-1}\mathcal{R}^{-2}\mathcal{F}_{|k|-1}\mathcal{B}_{|k|-1}\xi_k \tag{4.31}$$

$$\frac{d\xi_k}{dt} = \mathcal{R}^{-2}\mathcal{F}_{|k|-1}\mathcal{B}_{|k|-1}\xi_k \tag{4.32}$$

where the last step follows from the enforced artificial boundary condition $\xi \equiv 0$ for $r \geq R$. As $R \to \infty$, another justification of this step follows from the boundary conditions on ξ and the fact that the diffusion of

any bounded compactly supported initial vorticity distribution is so slow that $\mathcal{F}_{|k|}\omega_k(\rho)$ must remain zero at infinity over all finite subsequent time intervals.

We can also interpret the relationship between ψ, ξ and ω in terms of Cartesian coordinates.

COROLLARY 4.3. *Denoting the exterior points by Cartesian vectors* $\mathbf{x}$ *or* $\mathbf{y}$, *the following identities hold:*

$$\psi(\mathbf{x}) = \frac{1}{2\pi}\iint_{1\le|\mathbf{y}|\le|\mathbf{x}|} \xi(\mathbf{y})\,\frac{|\mathbf{x}|^2-|\mathbf{y}|^2}{|\mathbf{y}||\mathbf{x}-\mathbf{y}|^2}\,d\mathbf{y}^2 \tag{4.33}$$

$$\xi(\mathbf{x}) = -\frac{1}{2\pi}\iint_{|\mathbf{y}|\ge|\mathbf{x}|} \omega(\mathbf{y})\,\frac{|\mathbf{y}|^2-|\mathbf{x}|^2}{|\mathbf{x}||\mathbf{x}-\mathbf{y}|^2}\,d\mathbf{y}^2 \tag{4.34}$$

$$\xi(\mathbf{x}) = \frac{\partial\psi(\mathbf{x})}{\partial r} + \frac{1}{2\pi}\oint_{|\mathbf{y}|=|\mathbf{x}|} \frac{d^2\psi(\mathbf{y})}{ds^2}\,\log\left(\frac{|\mathbf{x}||\mathbf{y}|-\mathbf{x}\cdot\mathbf{y}}{2|\mathbf{x}||\mathbf{y}|}\right)ds \tag{4.35}$$

$$\omega(\mathbf{x}) = -\frac{\partial\xi(\mathbf{x})}{\partial r} - \frac{\xi(\mathbf{x})}{r} + \frac{1}{2\pi}\oint_{|\mathbf{y}|=|\mathbf{x}|} \frac{d^2\xi(\mathbf{y})}{ds^2}\,\log\left(\frac{|\mathbf{x}||\mathbf{y}|-\mathbf{x}\cdot\mathbf{y}}{2|\mathbf{x}||\mathbf{y}|}\right)ds \tag{4.36}$$

where $r = |\mathbf{x}|$ *and along the contour of integration* $\mathbf{y} = \mathbf{y}(s)$ *where* $s = r\theta$ *is the distance.*

The proof is based on theorems 4.1 and 4.2, and the observation that in Cartesian coordinates the functions g and h simplify to

$$g(\rho-\rho',\theta-\theta') = \frac{|\mathbf{x}|^2-|\mathbf{x}'|^2}{|\mathbf{x}-\mathbf{x}'|^2} \tag{4.37}$$

$$h(\theta-\theta') = \log\left(\frac{|\mathbf{x}||\mathbf{x}'|-\mathbf{x}\cdot\mathbf{x}'}{2|\mathbf{x}||\mathbf{x}'|}\right) \quad \text{along } |\mathbf{x}| = |\mathbf{x}'|. \tag{4.38}$$

We shall consider the pseudoenergy $\frac{1}{2}\|\xi\|^2$ as equivalent to the kinetic energy $\frac{1}{2}\|\mathbf{v}\|^2$. The following theorem shows that this is justified whenever $\psi(\rho,\theta)$ approaches a function of ρ alone as $\rho\to\infty$. This situation applies to flows of interest, whose initial vorticity distribution is compactly supported and total kinetic energy is finite.

THEOREM 4.4. *The total pseudoenergy is equal to the total kinetic energy and* $\|\xi\|^2 = \|\mathbf{v}\|^2$ *whenever the following sufficient condition holds:*

$$\lim_{r\to\infty}\int_0^{2\pi}\left|\frac{\partial\psi}{\partial\theta}\right|^2 d\theta = 0 \quad . \tag{4.39}$$

Proof:

$$\|\xi\|^2 = \int_0^\infty\int_0^{2\pi}\xi^2 r^2\,d\theta\,d\rho \tag{4.40}$$

$$= \int_0^\infty\int_0^{2\pi}|\mathcal{F}\psi|^2\,d\theta\,d\rho \tag{4.41}$$

$$= \int_0^\infty\sum_k\left(\left|\frac{d\psi_k}{d\rho}\right|^2 + k^2|\psi_k|^2 + |k|\left(\psi_k\frac{d\bar{\psi}_k}{d\rho} + \bar{\psi}_k\frac{d\psi_k}{d\rho}\right)\right)d\rho \tag{4.42}$$

$$= \int_0^\infty\int_0^{2\pi}|\mathbf{v}|^2 r^2\,d\theta\,d\rho + \sum_k|k||\psi_k|^2\Big|_{\rho=0}^{\infty} \tag{4.43}$$

$$= \|\mathbf{v}\|^2 \tag{4.44}$$

since at each ρ the infinite sum is bounded by

$$0 \le \sum_k|k||\psi_k|^2 \le \sum_k|ik\psi_k|^2 = \frac{1}{2\pi}\int_0^{2\pi}\left|\frac{\partial\psi}{\partial\theta}\right|^2 d\theta \tag{4.45}$$

which vanishes at $\rho = 0$ due to the boundary conditions and as $\rho \to \infty$ due the assumption of the theorem. Although an even milder assumption would suffice, we shall be satisfied with this result for the sake of simplicity.

5. Diagonalization of the ξ dynamics. At this point, we can solve the eigenvalue problem and obtain the modes of the pseudodifferential representation of the Stokes flow. First we shall consider a bounded computational domain, and then let $R \to \infty$ to include the full exterior domain.

On a bounded computational domain, system dynamics are governed by the operator defined by

$$\mathcal{A}_k f_k \stackrel{\text{def}}{=} \mathcal{R}^{-2} \mathcal{F}_{|k|-1} \mathcal{B}_{|k|-1} f_k \tag{5.1}$$

over the range $1 < r < R$ and 0 otherwise.

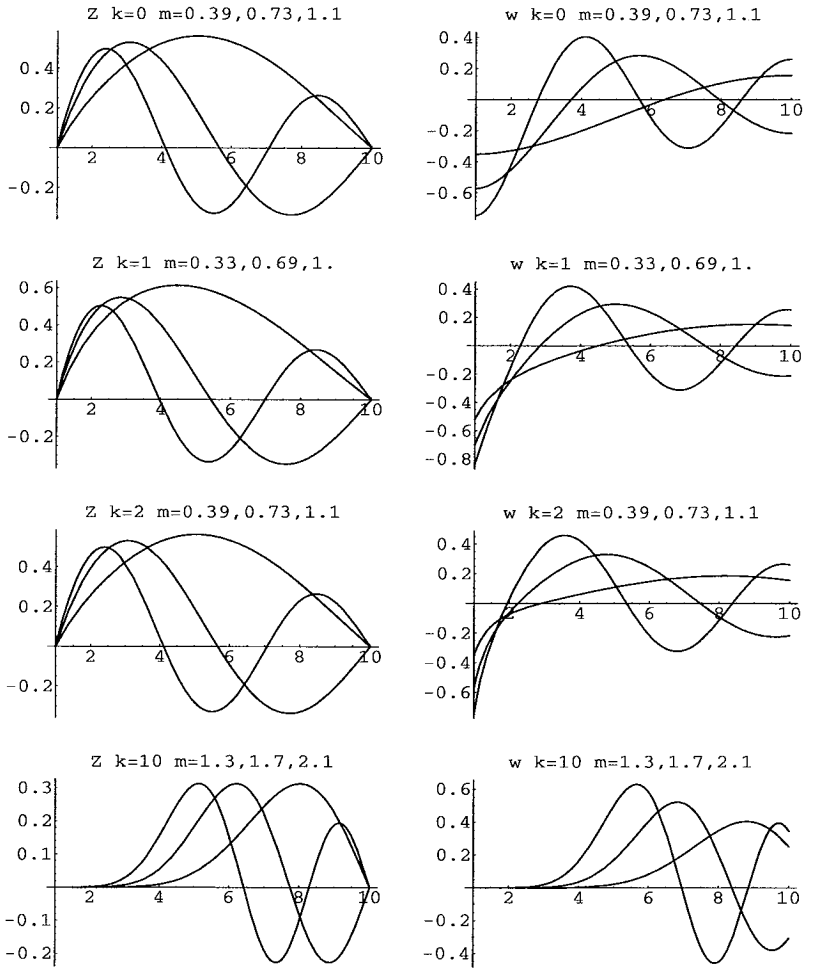

FIG. 5.1. *Typical modes of ξ (left) and ω (right) vs. radius.*

THEOREM 5.1. *The normalized solutions of the equation $(\mathcal{A}_k + m^2)\xi_k = 0$ restricted to the range*

$1 \le r \le R$ are linear combinations of the Bessel functions

$$Z_{nm}(r) = \frac{Y_n(mr)J_n(m) - J_n(mr)Y_n(m)}{\sqrt{J_n(m)^2 + Y_n(m)^2}} \tag{5.2}$$

where $n \stackrel{\text{def}}{=} ||k| - 1|$ and m is a root of the equation $Z_{nm}(1) = Z_{nm}(R) = 0$.

This theorem is proved by direct substitution. The operator $\mathcal{A}_k$ restricted to the interval $1 \le r \le R$ leads to the Bessel differential equation with Dirichlet boundary conditions, whose solutions are linear combinations of J_n and Y_n. This self adjoint Sturm-Liouville eigenvalue problem defines a complete family of eigenfunctions Z_{nm} which are orthogonal with respect to the weight function r:

$$\int_1^R r Z_{nm}(r) Z_{np}(r) dr = \frac{\delta_{mp}}{2m^2} \left(r \frac{dZ_{nm}(r)}{dr} \right)^2 \Bigg|_{r=1}^{R} . \tag{5.3}$$

For $m = p \gg n$ and large R, the asymptotic expansion

$$Z_{nm}(r) \sim \sqrt{\frac{2}{\pi m r}} \sin(m(r-1)) \tag{5.4}$$

applies and the integral (5.3) approaches $(R-1)/(\pi m)$. Moreover, all eigenvalues $-m^2$ are known to be real and strictly negative.

Figure 5.1 shows typical mode shapes of ξ and the corresponding ω modes. Vorticity modes for low $|k|$ exhibit a balance between vorticity creation at the wall and dissipation in the exterior domain. At high $|k|$, the time scales $m \ll |k|$ show no significant activity in vorticity at the wall where

$$\omega = \frac{-2/\pi}{\sqrt{J_n(m)^2 + Y_n(m)^2}} \sim \frac{-2(m/2)^n}{\Gamma(n)} \tag{5.5}$$

Due to the $\Gamma(n)$ term in the denominator, these vorticity modes are virtually unobservable at the wall. This has important implications for sensing.

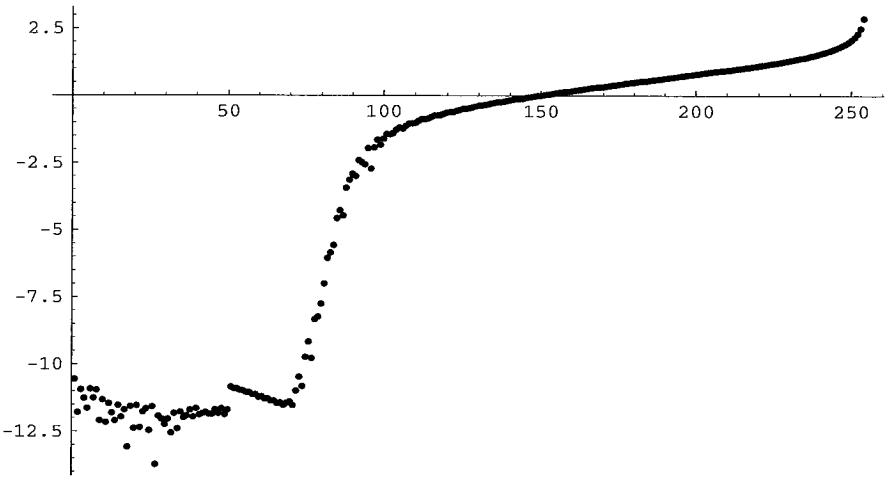

FIG. 5.2. *Comparison of numerical and analytic eigenvalues for $R = 100$ and $k = 0$. Logarithm (base 10) of the relative error is plotted. Virtually full machine accuracy is obtained up to the point of eigenfunction resolution failure near the 92nd eigenvalue. Chebyshev discretization of 257 points in the ρ direction was used.*

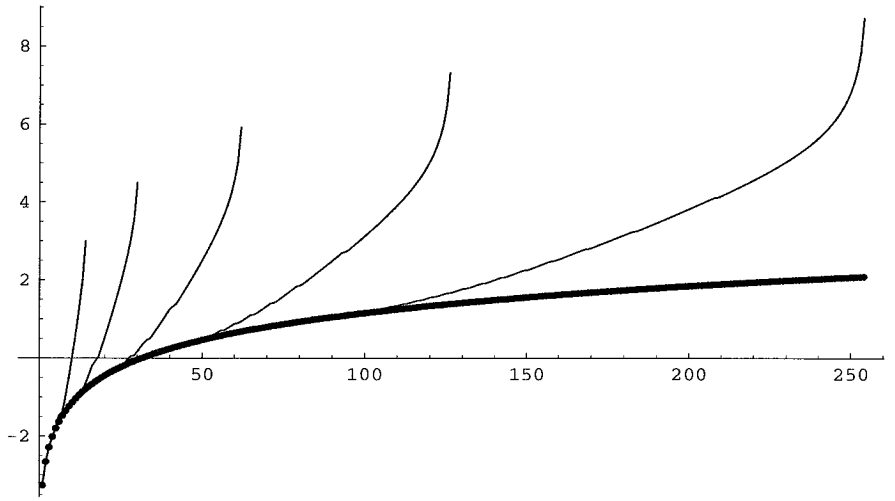

FIG. 5.3. *Logarithm (base 10) of the numerical eigenvalues computed at various resolutions (thin lines, $N = 17, 33, 65, 129, 257$) and the analytic eigenvalues (thick dots). Increasing the number of points helps delay resolution failure, which still limits the number of correctly computed eigenvalues.*

Comparing the analytic modes to the ones computed numerically using Fourier-Chebyshev spectral methods, we achieved nearly full machine accuracy for properly resolved eigenfunctions (figures 5.2, 5.3 and 5.4). As soon as the Nyquist criterion is violated *anywhere* in the domain, numerical eigenvalues exhibit nonphysical behavior. Those modes should be discarded as numerical artifacts. Care must be taken to construct discretizations which simultaneously resolve *all* eigenfunctions of interest.

The case $R \to \infty$ leads to a singular Sturm-Liouville eigenvalue problem. The system (4.23) may be diagonalized by means of Weber's transform [4]. This transform is a generalization of the Hankel transform. The relevant transform pair applied to a function $f(r)$, given our normalization of Z_{nm}, reads as follows:

$$F_m = \int_1^\infty f(r) Z_{nm}(r) r \, dr \stackrel{\text{def}}{=} \mathcal{W}_n f \tag{5.6}$$

$$f(r) = \int_0^\infty F_m Z_{nm}(r) m \, dm \stackrel{\text{def}}{=} \mathcal{W}_n^{-1} F \quad . \tag{5.7}$$

One may also show that Weber's transform satisfies a relation of the Parseval type:

$$\int_0^\infty F_m G_m m \, dm = \int_0^\infty F_m m \, dm \int_1^\infty g(r) Z_{nm}(r) r \, dr \tag{5.8}$$

$$= \int_1^\infty g(r) r \, dr \int_0^\infty F_m Z_{nm}(r) m \, dm \tag{5.9}$$

$$= \int_1^\infty f(r) g(r) r \, dr \quad . \tag{5.10}$$

A simple calculation shows that this transform diagonalizes $\mathcal{A}_k$ so that

$$\mathcal{W}_n \mathcal{A}_k \mathcal{W}_n^{-1} F_m = -m^2 F_m \tag{5.11}$$

and the ξ_k dynamics are described by

$$\Xi_{km} \stackrel{\text{def}}{=} \mathcal{W}_n \xi_k(r) \tag{5.12}$$

$$\frac{d\Xi_{km}}{dt} = -m^2 \Xi_{km} \quad . \tag{5.13}$$

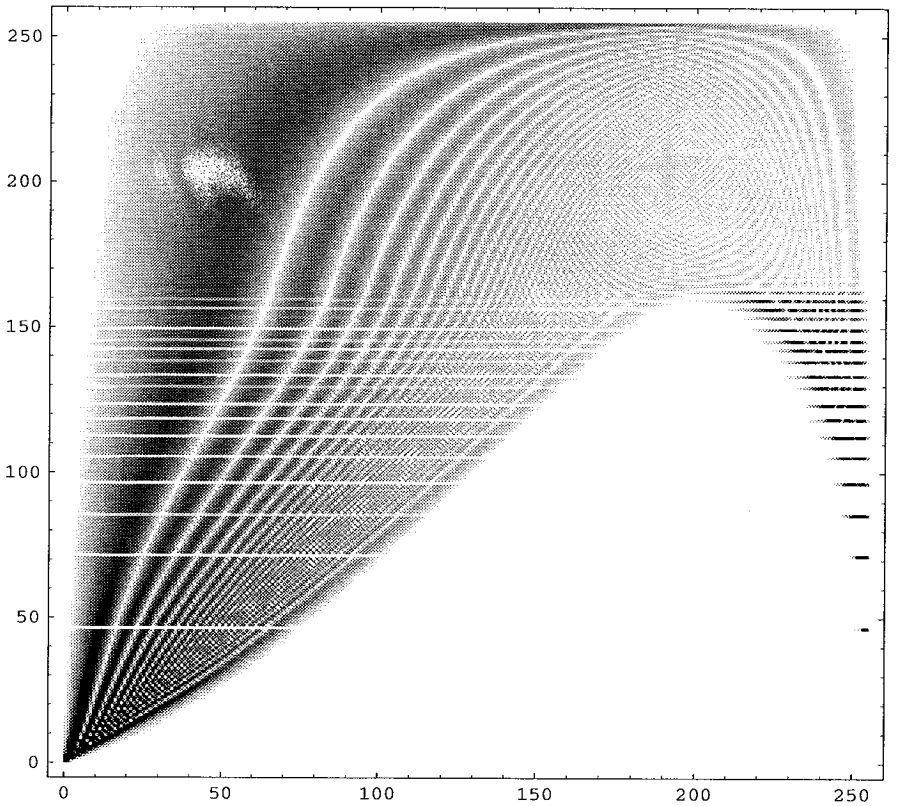

FIG. 5.4. *Plot density shows magnitude of numerically obtained modes from the least stable (top) to the most stable (bottom) for the circumferential wavenumber $k = 1$, using Chebyshev discretization in the ρ direction. There are 257 grid points from the cylinder wall at $r = 1$ (left) to the limit of the computational domain at $r = 100$ (right). The top portion is physically correct. Lower modes are numerical artifacts traced to the resolution failure starting near the gridpoint 200 of the eigenfunction shown at vertical coordinate 165, which corresponds to the 92nd eigenvalue.*

One also obtains a simple expression for the pseudoenergy of the flow represented by ξ:

$$\|\xi\|^2 \stackrel{\text{def}}{=} \int_1^\infty \int_0^{2\pi} \xi(r,\theta)^2 r \, d\theta \, dr = 2\pi \int_1^\infty \sum_{k=-\infty}^{\infty} |\xi_k(r)|^2 r \, dr \tag{5.14}$$

$$= 2\pi \sum_{k=-\infty}^{\infty} \int_0^\infty |\Xi_{km}|^2 m \, dm \quad . \tag{5.15}$$

6. Invariant subspaces and optimal control. We have shown that the system dynamics (4.23) may be diagonalized and that the invariant subspaces are of the form $e^{ik\theta} Z_{nm}(r)$ where $n = ||k| - 1|$ and $m > 0$. Moreover, the pseudoenergy form (5.14) is also simplified. This diagonalization leads to a family of optimal control problems which preserve the decomposition of the state space into invariant subspaces.

We shall seek to minimize the time integral of $\|\epsilon\xi\|^2 + \|u\|^2$, the weighted sum of the pseudoenergy norms of the flow state ξ and feedback u. By the diagonalization procedure described above, we are led to the 1-dimensional LQR control problem

$$\frac{d\Xi_{km}(t)}{dt} = -m^2 \, \Xi_{km}(t) + U_{km}(t) \tag{6.1}$$

$$\min_U \eta = m \int_0^\infty |\epsilon\, \Xi_{km}(t)|^2 + |U_{km}(t)|^2 dt \tag{6.2}$$

where $\epsilon > 0$ is a small gain parameter, $m > 0$ is real, and $\Xi_{km}(t)$ and $U_{km}(t)$ are complex scalars. The solution will be of the form $U_{km} = -K(m)\,\Xi_{km}$. Since m is real, the performance measure reads

$$\eta = \frac{m(\epsilon^2 + K(m)^2)}{2(K(m) + m^2)} |\Xi_{km}(0)|^2 \tag{6.3}$$

where $\Xi_{km}(0)$ is the initial state. Solving for the optimal $K(m)$ we obtain

$$K(m) = -m^2 + \sqrt{m^4 + \epsilon^2}. \tag{6.4}$$

This optimal functional gain achieves its maximum at $m = 0$ and behaves as follows:

$$K(m) = \begin{cases} \epsilon + O(m^2) & \text{for } m \ll \sqrt{\epsilon} \\ \epsilon(\sqrt{2} - 1) & \text{for } m = \sqrt{\epsilon} \\ \epsilon^2/(2m^2) + O(\epsilon^4/m^6) & \text{for } m \gg \sqrt{\epsilon}\,. \end{cases} \tag{6.5}$$

The optimal feedback law in Ξ representation is $U_{km}(t) = -K(m)\Xi_{km}(t)$. The optimal performance measure is $\eta = m\,K(m)|\Xi_{km}(0)|^2$.

6.1. Rational approximation of optimal feedback. While the above explicit solutions give the optimal feedback, their analytic form is complicated. Fortunately, the performance criterion is not very sensitive to perturbations in the optimal control. We may replace the optimal gain $K(m)$ by a simple rational approximation while increasing the corresponding performance measure η only slightly.

Consider $K_1(m) = \epsilon^2/(2m^2 + \epsilon)$ as the rational approximation to the optimal feedback. This expression matches the behavior of $K(m)$ as $m \to \infty$ and reaches the same value at $m = 0$. The maximum absolute error in gain is 0.121585ϵ, reached at $m = 0.617541\sqrt{\epsilon}$. However, the maximum relative error in optimality is

$$\frac{\eta_1(m) - \eta(m)}{\eta(m)} = \frac{\epsilon^2\,\sqrt{\epsilon^2 + m^4}\,\left(\epsilon^2 + 2\,\epsilon\,m^2 + 2\,m^4\right)}{(\epsilon + 2\,m^2)\,\left(\epsilon^2 + \epsilon\,m^2 + 2\,m^4\right)\,\left(\epsilon^2 + m^4 - m^2\,\sqrt{\epsilon^2 + m^4}\right)} - 1 \tag{6.6}$$

and its maximum of 0.0114695 (less than 1.147 percent) is reached at $m = 0.658911\sqrt{\epsilon}$. At other values of m the relative error in optimality is even smaller, and typical relative loss in performance will be only one percent or less. By contrast, the relative performance loss without any feedback tends to infinity as $m \to 0$.

The advantage of using the slightly suboptimal gain K_1 is that this rational function may be immediately linked to the resolvent of the original operator (with the same boundary conditions). The sequence of transformations may then be inverted to conclude that the following theorem holds:

THEOREM 6.1. *Given a diagonalizable operator $\mathcal{A}$ such that its spectrum is real and negative, and a simultaneously diagonalized performance measure η of type (6.2), the suboptimal feedback kernel*

$$\mathcal{K}_1 = \epsilon^2\,(\beta\epsilon\mathcal{I} - 2\mathcal{A})^{-1}\,. \tag{6.7}$$

where $\beta = 1$ results in worst case performance loss of 1.14695 percent relative to the optimal feedback kernel. Denoting by $-m^2$ the eigenvalues of $\mathcal{A}$, the worst case occurs at $m = 0.658911\sqrt{\epsilon}$. The worst case relative performance loss is reduced to 0.6437126 percent when $\beta = 0.89279$ but it occurs at both $m = 0$ and $m = 0.748032\sqrt{\epsilon}$.

The generalization $\beta \neq 1$ is obvious, and its optimal value reported above was obtained numerically. Unless otherwise stated, we shall be using the value $\beta = 1$.

A better approximation would express the optimal gain as a sum of different resolvents. The following theorem shows how this can be done.

THEOREM 6.2. *When $z = \sqrt{i/2}$ and p is real and positive, the expression*

$$\frac{1}{2}\left(\frac{z}{z+p} + \frac{\bar{z}}{\bar{z}+p}\right) \tag{6.8}$$

approximates $\sqrt{p^2+1} - p$ with worst case absolute error of -0.0182787 at $p = 0.571448$ and worst case relative error of -3.48583 percent at $p = 0.854638$.

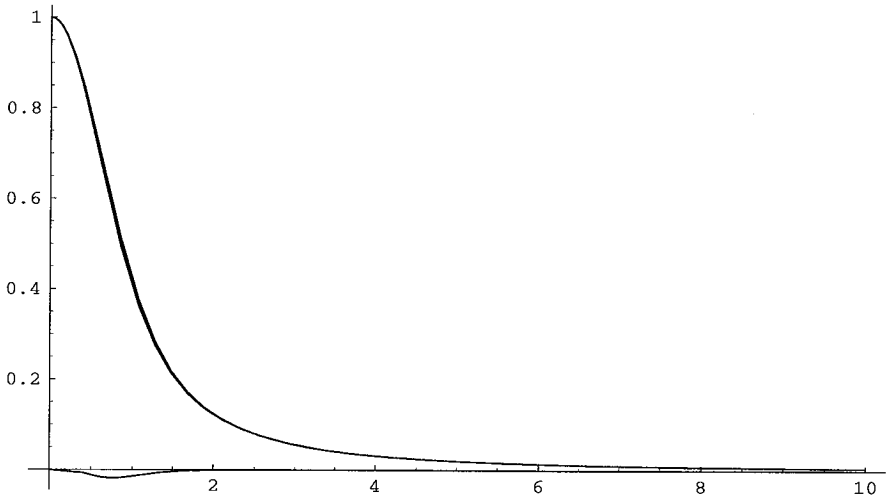

FIG. 6.1. *Exact gain, its rational approximation (6.8) and their difference plotted as a function of $\sqrt{p}$. The approximation underestimates the exact value only slightly, by less than 3.5 percent.*

It is useful to note that this approximation can be written as $\Re[z/(z+p)]$. Further calculations demonstrate that the worst case relative performance loss is 0.0256434 percent, reached at $p = 0.617808$ (figure 6.1). Taking p to be the eigenvalue of $-\mathcal{A}/\epsilon$, we obtain the corresponding approximate feedback kernel as a sum of two Green's functions:

$$\mathcal{K}_2 = \frac{\epsilon}{2}\left(\epsilon z\left(\epsilon z\mathcal{I} - \mathcal{A}\right)^{-1} + \epsilon\bar{z}\left(\epsilon\bar{z}\mathcal{I} - \mathcal{A}\right)^{-1}\right) \tag{6.9}$$

$$= \epsilon\,\Re\left[\epsilon z\left(\epsilon z\mathcal{I} - \mathcal{A}\right)^{-1}\right]. \tag{6.10}$$

These results will be used to derive analytic approximations to the optimal feedback operator.

6.1.1. A simple example of rational approximation. The heat equation on an infinite line is $h_t = h_{xx}$ and can be diagonalized by Fourier transform so that $\hat{h}_t = -k^2\hat{h}$. For this simple example, the spatial representation of the optimal feedback kernel can be obtained analytically [16] in terms of the generalized hypergeometric function ${}_0F_3$. The exact expression for the optimal control is $u(x) = -\int \kappa(x,x')h(x')dx'$ where

$$\kappa(x,x') = -\left(\epsilon/\pi\right)^{3/2}\left(\frac{1}{2}\Gamma\left(-\frac{3}{4}\right)\Gamma\left(\frac{5}{4}\right){}_0F_3\left(;\frac{1}{2},\frac{3}{4},\frac{7}{4};-s^4\right) -\right.$$

$$s^2\Gamma\left(-\frac{5}{4}\right)\Gamma\left(\frac{3}{4}\right)\,{}_0F_3\left(;\frac{5}{4},\frac{3}{2},\frac{9}{4};-s^4\right)+$$

$$|s|\pi^{3/2}\,{}_0F_3\left(;\frac{3}{4},\frac{5}{4},2;-s^4\right)\Big) \tag{6.11}$$

where we have defined $s=(x-x')\sqrt{\epsilon}/4$. The two rational approximations defined above evaluate to

$$\kappa_1(x,x') = (\epsilon/2)^{3/2}\,e^{-2\sqrt{2}\,|s|} \tag{6.12}$$

and

$$\kappa_2(x,x') = \sqrt{\frac{\epsilon^3}{4\sqrt{2}}}\,e^{-|s|\,2\sqrt{\sqrt{2}+1}}\,\cos\left(\frac{\pi}{8}-|s|\,2\sqrt{\sqrt{2}-1}\right). \tag{6.13}$$

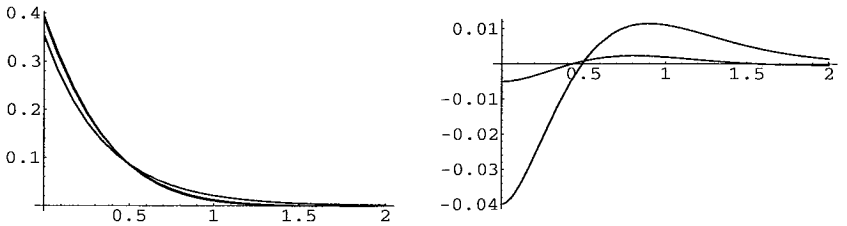

FIG. 6.2. *Spatial form of the optimal feedback kernel for the heat equation on an infinite line. Left: the exact κ (6.11) and its rational approximations κ_1 and κ_2 as functions of s for $\epsilon=1$. Right: error in the two rational approximations shown using expanded vertical scale. See text.*

For both rational approximations the maximum error occurs at $s=0$ (figure 6.2). The exact value of the feedback kernel at $s=0$ should be $-(\epsilon/\pi)^{3/2}\Gamma(-3/4)\Gamma(5/4)/2$. By comparison, κ_1 gives a 10.14 percent lower value while κ_2 underestimates by only 1.27 percent. We have already shown that both of these suboptimal strategies perform nearly as well as the optimal control. In spectral representation, the corresponding worst case relative performance losses are less than 1.147 percent and less than 0.026 percent, respectively.

We note that the κ_2 exhibits sign changes starting at $s=5\pi\sqrt{\sqrt{2}+1}/16\approx 1.52541$. This is qualitatively correct since the exact feedback kernel κ also exhibits sign changes (spaced by approximately 1.12 at first) starting at $s\approx 1.47894$. The magnitude of the feedback kernel beyond that point is at most $0.000334\epsilon^{3/2}$ so this interesting behavior has little bearing on the form of the optimal feedback.

6.1.2. Rational approximation and 2D diffusion. Consider the heat equation in an infinite plane: $h_t=\Delta h$. While the exact spatial form of the optimal feedback kernel could not be obtained analytically, rotational symmetry leads to the rational approximations

$$\kappa_1(\mathbf{x},\mathbf{x}') = \frac{\epsilon^2}{4\pi}K_0\left(r\sqrt{\frac{\epsilon}{2}}\right) \tag{6.14}$$

and

$$\kappa_2(\mathbf{x},\mathbf{x}') = \frac{\epsilon^2}{4\pi}\left(\frac{1+i}{2}K_0\left(r\sqrt{\frac{(1+i)\epsilon}{2}}\right)+\frac{1-i}{2}K_0\left(r\sqrt{\frac{(1-i)\epsilon}{2}}\right)\right) \tag{6.15}$$

where the distance between the points in the plane $\mathbf{x}$ and $\mathbf{x}'$ defines $r=|\mathbf{x}-\mathbf{x}'|$. These expressions involve the modified Bessel function K_0, which has a logarithmic singularity at $r=0$. The difference between these

two approximations approaches its maximum as r tends to zero:

$$\lim_{r\to 0}(\kappa_2-\kappa_1)=\frac{\epsilon^2(\pi-2\log(2))}{32\pi} \approx 0.0174603\epsilon^2 \quad . \tag{6.16}$$

6.1.3. Rational approximation and 3D diffusion. For the heat equation in 3D free space, the rational approximations yield

$$\kappa_1(\mathbf{x},\mathbf{x}')=\frac{\epsilon^2}{8\pi r}e^{-r\sqrt{\epsilon/2}} \tag{6.17}$$

and

$$\kappa_2(\mathbf{x},\mathbf{x}')=\frac{\epsilon^2}{4\sqrt{2}\pi r}e^{-r\sqrt{\epsilon(1+\sqrt{2})}/2}\cos\left(\frac{\pi}{4}-\frac{r}{2}\sqrt{\epsilon(\sqrt{2}-1)}\right) \tag{6.18}$$

where $r=|\mathbf{x}-\mathbf{x}'|$ is the distance between the two points in space. The origin $r=0$ is now a simple pole, where the difference between these two approximations approaches its maximum given by

$$\lim_{r\to 0}(\kappa_2-\kappa_1)=\frac{\epsilon^{5/2}\left(1+\sqrt{\sqrt{2}-1}\right)}{8\sqrt{2}\pi} \approx 0.0462423\epsilon^{5/2} \quad . \tag{6.19}$$

7. Approximately optimal control of Stokes flow. To obtain the rational approximation of the optimal feedback kernel for equation (4.23), we first need to determine the Green's function which solves the auxiliary problem

$$\epsilon z\mu_k-\Delta_n\mu_k=\epsilon z\xi_k \tag{7.1}$$

where $n=||k|-1|$ and Dirichlet boundary conditions are applied.

The required Green's function can be derived explicitly in terms of modified Bessel functions

$$G_n(r,s)=a^2\left(I_n(a\min(r,s))K_n(a\max(r,s))-\frac{K_n(ar)K_n(as)I_n(a)}{K_n(a)}\right) \tag{7.2}$$

where $a=\sqrt{\epsilon z}$. The solution can now be written as

$$\mu_k(r)=\int_1^\infty G_n(r,s)\xi_k(s)s\,ds \tag{7.3}$$

where μ_k and ξ_k are now expressed as functions of the radius. The rational approximations to the optimal feedback kernel are obtained in terms of G_n.

From now on, we shall focus on the case $z=\sqrt{\pm i/2}$ and refer to the resulting approximate kernel of type (6.9) as simply $\tilde{\kappa}$.

THEOREM 7.1. *The rational approximation of type (6.9) to the optimal feedback kernel for the system governed by (4.23) is given by*

$$\tilde{\kappa}_k(r,s)=\epsilon\Re\left[G_n(r,s)\right] \quad \text{using } a=\sqrt{\epsilon\sqrt{i/2}} \tag{7.4}$$

where $n=||k|-1|$ and $G_n(r,s)$ is defined by (7.2) for the indicated value of a.

These feedback kernels exhibit a pronounced ridge along the line $r=s$ representing colocated sensing and actuation. Figure 7.1 shows the typical form of control laws derived from feedback kernels $\tilde{\kappa}_k$. The colocated

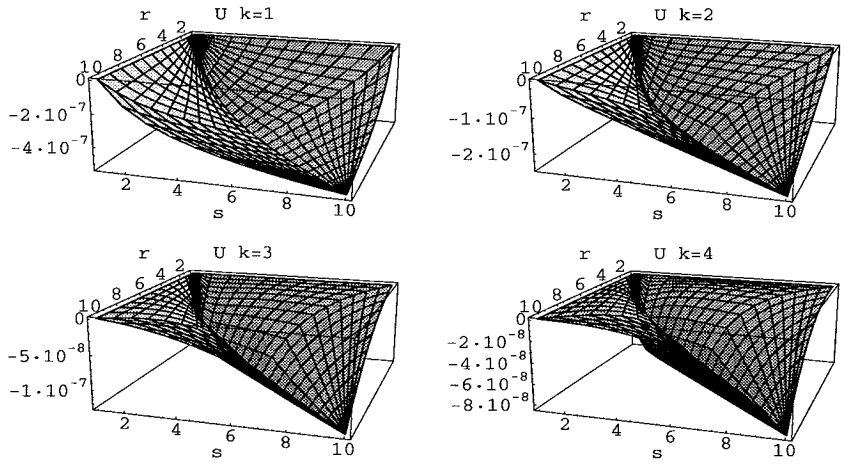

FIG. 7.1. *Feedback at r due to disturbance in ξ_k at s for $\epsilon = 0.001$ and $k = 1, \ldots, 4$.*

control ridge becomes essentially flat for large $|k|$. However, this feedback gain does not yet provide spatial clues because it is expressed in our nonlocal pseudodifferential representation. The spatial information we seek involves returning to the vorticity representation. This can be done as follows.

We shall assume that the gain parameter ϵ is small and consider disturbances ξ_k whose support is contained within a finite computational domain of size $R \ll 1/|a|$. Under these conditions, $|a \max(1, r, s)| \ll 1$ and the Green's function behaves as

$$G_n(r,s) \sim \frac{a^2 \left(\min(r,s)^n - \min(r,s)^{-n}\right)}{2n \, \max(r,s)^n} \tag{7.5}$$

when $n \neq 0$. This applies when $k \neq \pm 1$ and we obtain

$$\tilde{\kappa}_k(r,s) \sim \frac{\epsilon^2 \left(\min(r,s)^n - \min(r,s)^{-n}\right)}{4n \, \max(r,s)^n} \stackrel{\text{def}}{=} \tilde{\lambda}_k(r,s) \; . \tag{7.6}$$

For the special case $n = 0$, we obtain the expression

$$G_0(r,s) \sim a^2 \log(\min(r,s)) \left(1 + \frac{\log(\max(r,s))}{\gamma + \log(a/2)}\right) \tag{7.7}$$

where $\gamma \approx 0.577216$ is Euler's constant gamma. The term $\log(a/2)$ evaluates to $\log(\epsilon)/2 - 5\log(2)/4 \pm i\pi/8$ when $z = \sqrt{\pm i/2}$. After some algebra, we obtain

$$\tilde{\kappa}_{\pm 1}(r,s) \sim \frac{\epsilon^2 \log(\min(r,s))}{2} \left(1 + \alpha \, \log(\max(r,s))\right) \stackrel{\text{def}}{=} \tilde{\lambda}_{\pm 1}(r,s) \tag{7.8}$$

where α is defined by (7.13).

The asymptotic form of $\tilde{\kappa}$ will constitute our *low gain rational approximation* (denoted by $\tilde{\mathcal{L}}$ and considered an integral operator with kernel $\tilde{\lambda}(r,s)$) which is applicable within the domain of radius $R \ll 1/\sqrt{\epsilon}$. The approximately optimal control in pseudodifferential representation is $-\tilde{\mathcal{L}}\xi$, but to get its spatial interpretation we must go back to the vorticity representation, where $\tilde{\mathcal{L}}_k$ is transformed to

$$\mathcal{L}_k = \mathcal{R}^{-1} \mathcal{B}_{|k|-1} \tilde{\mathcal{L}}_k \mathcal{B}_{|k|-1}^{-1} \mathcal{R} \; . \tag{7.9}$$

THEOREM 7.2. *The low gain rational approximation to the optimal feedback kernel in vorticity representation is given by*

$$\lambda_0(r,s) = \epsilon^2 \log\left(\min(r,s)/s\right)/2 \tag{7.10}$$

$$\lambda_{\pm 1}(r,s) = \epsilon^2 \left(2\min(r,s)^2 - s^2(2\alpha\log(s) - \alpha + 2) - \alpha\right)/(8rs) \tag{7.11}$$

$$\lambda_k(r,s) = \epsilon^2 \left(\min(r,s)^{2|k|} - |k|s^2 + |k| - 1\right) / \left(4|k|(rs)^{|k|}\right) \tag{7.12}$$

where $|k| \geq 2$ *and the parameter* α *is given by*

$$\alpha = \frac{8(\pi + 8\gamma + 2\log(\epsilon^2/32))}{\pi^2 + (8\gamma + 2\log(\epsilon^2/32))^2}. \tag{7.13}$$

This approximation applies within the domain of radius $R \ll 1/\sqrt{\epsilon}$.

We note that if the support of ω_k is contained within a computational domain of radius R, so is the support of ξ_k and therefore the low gain approximation remains valid. One must also make a distinction between $|k| - 1$ and $n = ||k| - 1|$, and pay attention to the limits of integration. Once that is done, the theorem follows by a straightforward but lengthy calculation.

This result is given as a function of radius and the nearly optimal control law now reads

$$u_k(r) = -\int_1^\infty \lambda_k(r,s)\omega_k(s)sds\ . \tag{7.14}$$

As we have shown before, the maximum relative error of the rational approximation $\mathcal{K}_2$ is under 3.5 percent, resulting in maximum relative performance loss of under 0.026 percent. The kernel $\lambda_k(r,s)$ also involves the low gain approximation, where the neglected term is of relative order $O(\epsilon)$. Since we expect that ϵ is in the range of 1 percent or less, $\lambda_k(r,s)$ is an excellent approximation to the exact optimal distributed feedback. Using $\epsilon = 0.001$ and $R = 10$, the maximum relative error of the low gain approximation remains under 2 percent.

7.1. How to control a particular vortex. We shall assume that a resolution limit on control and observation exists, so that only the subsystems $|k| \leq K$ need to be considered. This assumption suggests an evaluation of the control effort at each wavenumber.

Given a vorticity distribution ω which satisfies integral compatibility constraints, we shall focus at the contribution of the vorticity near $(r,\theta) = (s,\phi)$. Consider a particular vortex of the form $\omega(r,\theta) = \delta(r-s)\delta(r(\theta-\phi))$ whose Fourier transform yields

$$\omega_k(r) = \frac{\delta(r-s)}{2\pi s} e^{-ik\phi}\ . \tag{7.15}$$

For simplicity, we shall take $\phi = 0$ and consider the distributed feedback produced by the low gain rational approximation. This single vortex in the flow induces a vortex sheet at the solid boundary, which does not contribute to the control because the feedback kernel is zero for vortices at the boundary.

Distributed vorticity control (Fig. 7.2) exhibits two pronounced ridges within the bounded domain where our low gain rational approximation applies.

The ridge along the line $r = s$ represents the colocated control. Within the region of radius $R \ll 1/\sqrt{\epsilon}$ this control is zero for $k = 0$, grows logarithmically with r for $|k| = 1$, and saturates at a fixed value proportional to $1/|k|$ for $|k| \geq 2$. This control represents colocated vorticity damping, opposing the disturbance vortex.

Another ridge is present along the solid boundary. The magnitude of this control grows logarithmically with s for $k = 0$, behaves as $s\log(s)$ for $|k| = 1$ and as $s^{-|k|}(s^2 - 1)$ for $|k| \geq 2$. This form of control creates a vortex at the wall of the *same* orientation as the disturbance vortex.

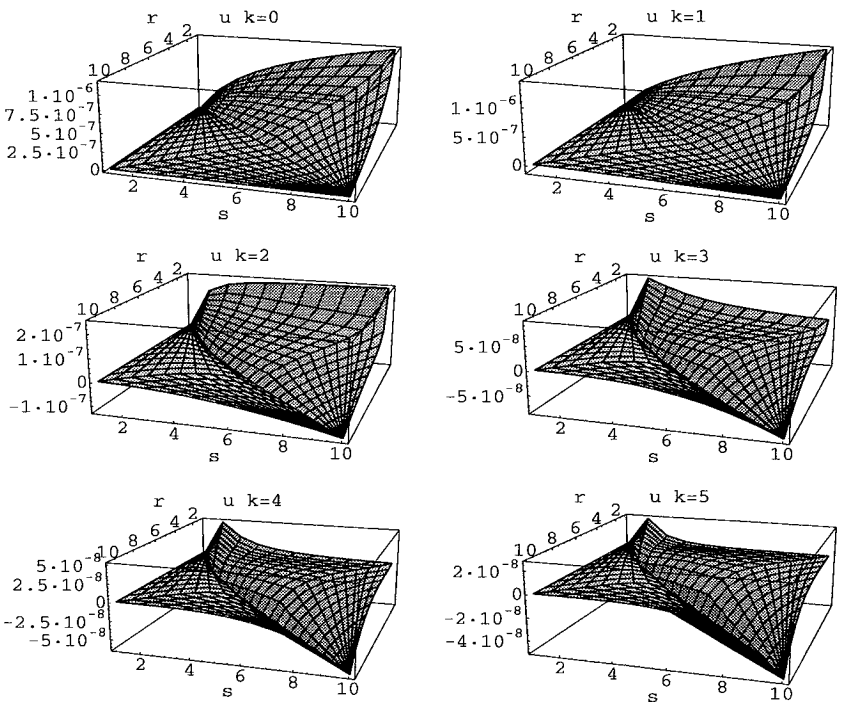

FIG. 7.2. *Distributed vorticity control at r in response to a vortex at s for $\epsilon = 0.001$ and $k = 0, \ldots, 5$. Boundary control and colocated control dominate.*

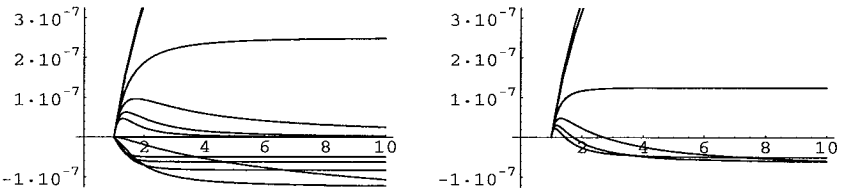

FIG. 7.3. *Left: Boundary control (positive traces) and colocated control (negative traces) as functions of the radial location of the disturbance vortex for $\epsilon = 0.001$ and $k = 0, \ldots, 5$. Right: Sum of boundary control and colocated control. Within the region $R \ll 1/\sqrt{\epsilon}$, boundary control dominates for $|k| \leq 2$ or sufficiently close to the wall.*

Figure 7.3 demonstrates that for $|k| \leq 2$ more control is applied at the boundary than at the vortex location (within the region where low gain approximation holds). For $|k| \geq 3$, boundary control still dominates within a thin layer along the boundary, but colocated control is preferred in the rest of the domain. Using the low gain approximation, analysis and numerical experiments indicate that for $|k| \geq 3$ the region of boundary control dominance does not depend on ϵ and extends to

$$s = p + q\sqrt{\frac{1 - p^{|k|} + |k|(p^2 - 1)}{|k|(|k| - 2)}} \tag{7.16}$$

where $p = 2^{1/(|k|-2)}$ and $q \approx 0.9 \pm 0.01$.

Although boundary control dominates for low $|k|$ and near the solid boundary, the control input depends

on the vorticity distribution within the flow. Vorticity at the wall has *zero* impact on the control. Therefore, sensing vorticity at the wall is not directly useful. One must estimate the flow state away from the wall.

8. Conclusions. The analytic expressions we obtained were used to validate a numerical scheme based on Fourier-Chebyshev spectral methods. While full accuracy was achieved for properly resolved eigenfunctions, numerical artifacts were observed in other cases. This reinforces the obvious but important point that the chosen discretization must simultaneously resolve all eigenfunctions of interest throughout the computational domain.

The analytic form of the approximately optimal feedback shows that boundary control dominates for $|k| \leq 2$ or when the vorticity disturbance is sufficiently close to the wall. We obtained explicit estimates on the distance from the wall within which the optimal control favors actuation by means of boundary vortex generators.

We have also shown that vorticity at the wall does not influence the optimal control. The control effort depends on estimating the flow state away from the wall. This is a dual problem to the results reported here. The mode shapes in vorticity representation show that some modes are virtually unobservable at the wall, leading to limits on the effectiveness of boundary sensing. In future work, we hope to report on the estimation problem, and to extend this approach to more complex flows.

REFERENCES

[1] J. A. Burns and B. B. King, *A note on the regularity of solutions of infinite dimensional Riccati equations*, ICASE Report 94-20, ICASE, Hampton, VA, 1994.

[2] R. F. Curtain, *Spectral systems*, International Journal of Control, 39 (1984), pp. 657–666.

[3] R. F. Curtain and K. Glover, *Controller design for distributed systems based on Hankel-norm approximations*, IEEE Transactions on Automatic Control, AC-31 (1986).

[4] B. Davies, *Integral Transforms and their Applications*, Springer-Verlag, New York, 1985.

[5] A. El Jai and A. J. Pritchard, *Sensors and actuators in distributed systems*, International Journal of Control, 46 (1987), pp. 1139–1153.

[6] A. El Jai, M. S. Simon, E. Zerrik, and A. J. Pritchard, *Regional controllability of distributed parameter systems*, International Journal of Control, 62 (1995), pp. 1351–1365.

[7] U. Frisch, *Turbulence: The Legacy of A. N. Kolmogorov*, Cambridge University Press, Cambridge, 1995.

[8] J. A. Lewis and G. F. Carrier, *Some remarks on the flat plate boundary layer*, Quarterly of Applied Mathematics, 7 (1949), pp. 228–234.

[9] M. J. Lighthill, *Introduction. Boundary layer theory*, in Laminar Boundary Layers, L. Rosenhead, ed., Oxford University Press, London, 1963.

[10] K. B. Lim, *Method for optimal actuator and sensor placement for large flexible structures*, Journal of Guidance, Control and Dynamics, 15 (1992), pp. 49–57.

[11] S. L. Padula and R. K. Kincaid, *Aerospace applications of integer and combinatorial optimization*, NASA Technical Memorandum 110210, NASA Langley Research Center, 1995.

[12] A. D. Rubio, *Distributed Parameter Control of Thermal Fluids*, PhD thesis, Virginia Polytechnic Institute and State University, Blacksburg, VA, 1997. ICAM Report 97-04-01.

[13] R. Temam, *Navier-Stokes Equations*, North-Holland, Amsterdam, 1984.

[14] S. V. Tsynkov, *An application of nonlocal external conditions to viscous flow computations*, Journal of Computational Physics, 116 (1995), pp. 212–225.

[15] J. T. Wloka, B. Rowley, and B. Lawruk, *Boundary Value Problems for Elliptic Systems*, Cambridge University Press, Cambridge, 1995.

[16] Wolfram Research, Inc., *Mathematica 3.01*, 1996.

REPORT DOCUMENTATION PAGE

Form Approved
OMB No. 0704-0188

1. AGENCY USE ONLY *(Leave blank)*	2. REPORT DATE	3. REPORT TYPE AND DATES COVERED
	May 1998	Contractor Report

4. TITLE AND SUBTITLE
Optimal Control of Unsteady Stokes Flow Around a Cylinder and the Sensor/Actuator Placement Problem

5. FUNDING NUMBERS
C NAS1-19480
C NAS1-97046
WU 505-90-52-01

6. AUTHOR(S)
Josip Loncaric

7. PERFORMING ORGANIZATION NAME(S) AND ADDRESS(ES)
Institute for Computer Applications in Science and Engineering
Mail Stop 403, NASA Langley Research Center
Hampton, VA 23681-2199

8. PERFORMING ORGANIZATION REPORT NUMBER
ICASE Report No. 98-18

9. SPONSORING/MONITORING AGENCY NAME(S) AND ADDRESS(ES)
National Aeronautics and Space Administration
Langley Research Center
Hampton, VA 23681-2199

10. SPONSORING/MONITORING AGENCY REPORT NUMBER
NASA/CR-1998-207680
ICASE Report No. 98-18

11. SUPPLEMENTARY NOTES
Langley Technical Monitor: Dennis M. Bushnell
Final Report
To appear in the Proceedings of the AFOSR Workshop on Optimal Design and Control.

12a. DISTRIBUTION/AVAILABILITY STATEMENT
Unclassified–Unlimited
Subject Category 64, 34
Distribution: Nonstandard
Availability: NASA-CASI (301)621-0390

12b. DISTRIBUTION CODE

13. ABSTRACT *(Maximum 200 words)*
Effective placement of sensors and actuators is of crucial importance in flow control. Instead of using combinatorial search to identify optimal locations, we pose a related problem of polynomial complexity. If one could sense everything and actuate everywhere, what should one do? Using the unsteady 2D Stokes flow around a cylinder as an example, we obtain the analytic solution of an optimal distributed control problem and describe its spatial structure. At low circumferential wavenumbers or close to the cylinder wall, boundary vortex generators are shown to be more effective than colocated vorticity damping. This analytic solution has also been used to test numerical methods, demonstrating the importance of using discretization which resolves all eigenfunctions of interest.

14. SUBJECT TERMS
optimal flow control; exterior Stokes flow; sensor/actuator placement; design

15. NUMBER OF PAGES
23

16. PRICE CODE
A03

17. SECURITY CLASSIFICATION OF REPORT	18. SECURITY CLASSIFICATION OF THIS PAGE	19. SECURITY CLASSIFICATION OF ABSTRACT	20. LIMITATION OF ABSTRACT
Unclassified	Unclassified		